

# **Robust gold nanoparticles stabilized by trithiols for application in chemiresistive sensors**

Niti Garg<sup>1†</sup>, Ashok Mohanty<sup>1†</sup>, Nathan Lazarus<sup>2</sup>, Lawrence Schultz<sup>3</sup>, Tony R. Rozzi<sup>4</sup>, Suresh Santhanam<sup>2</sup>, Lee Weiss<sup>3</sup>, Jay L. Snyder<sup>4</sup>, Gary K. Fedder<sup>3,4</sup>, and Rongchao Jin<sup>1\*</sup>

<sup>1</sup>*Department of Chemistry, Carnegie Mellon University, Pittsburgh, PA 15213*

<sup>2</sup>*Department of Electrical and Computer Engineering, Carnegie Mellon University, Pittsburgh, PA 15213*

<sup>3</sup>*The Robotics Institute, Carnegie Mellon University, Pittsburgh, PA 15213*

<sup>4</sup>*National Institute for Occupational Safety and Health (NIOSH), Pittsburgh, PA 15236*

## **Abstract**

The use of metal nanoparticles (e.g. Au) coated with an organic monolayer of thiol for application in chemiresistive sensors was initiated in late 1990s; since then such type of sensors have been widely pursued due to their high sensitivities and reversible responses to volatile organic compounds (VOCs). However, a major issue for chemical sensors based on thiol-capped gold nanoparticles is their poor long-term stability as a result of slow degradation of the monothiol-to-gold bonds. We have devised a strategy to overcome this limitation by synthesizing a more robust system using Au nanoparticles capped by trithiol ligands. Compared to their monothiol counterpart, the new system is significantly more stable and also shows improved sensitivity towards different types of polar or non-polar VOCs. Thus, the trithiol-Au nanosensor holds great promise for the use in real world applications.

Keywords: Gold, trithiol, nanoparticle, chemiresistive, sensor

† These authors contribute equally.

\*Address for correspondence: Carnegie Mellon University, Department of Chemistry, Pittsburgh, Pennsylvania 15213, USA. *Email: rongchao@andrew.cmu.edu*

## 1. Introduction

The development of cost-effective, microminiature gas chemical sensors that exhibit fast response time and have high sensitivity and selectivity has long been a major pursuit of nanoscience and nanotechnology [1-5]. The use of nanoparticle materials, with scale of a few nanometers to approximately 100 nm, has enabled new types of sensors that are capable of detecting extremely small amounts of analytes such as chemical vapors in the range of few ppm. Among the various sensing techniques, chemiresistive sensors based on nanoparticle/polymer thin films, which consist of networks of nanoparticles cores surrounded by organic moiety show great promise due to their low power consumption, simplicity in fabrication and operation, and their potential for reliable detection [6-10]. When a thin film absorbs gas molecules, the electrical resistance of the film changes, which can be used for qualitative or quantitative analysis to detect the presence, type, and amount of analytes. In recent years, chemiresistive sensors based upon thin films of phthalocyanine, conjugated polymers, or carbon nanotubes have been developed to detect a wide range of vapor analytes [11-13]. Early research on gold nanoparticle-based chemiresistors dates back to 1998 when Wohltjen and Snow were the first who demonstrated a type of chemical vapor sensor using alkanethiol-protected gold nanoparticles as the sensing material [14]. The stability, reproducibility, and processibility of these sensors were found to be superior compared with other existing systems and hence, extensive work has been reported since then to further develop this type sensor [15-20].

When an Au nanoparticle thin-film sensor is exposed to organic vapors, sorption of vapor molecules into the organic film causes it to swell, resulting in an increase in the distances between the nanoparticles, leading to changes in the film's electrical impedance. The mechanism of charge transport between the nanoparticles is generally believed to be electron tunneling between metal cores and electron hopping along the alkanethiolate chains. Consequently, the current decreases as the film swells [21-23]. The conductivity ( $\sigma$ ) of the nanoparticle film at temperature  $T$  is described by the relation [24]

$$\sigma = \exp(-\beta s) \exp\left(-\frac{E_c}{k_B T}\right) \quad (1)$$

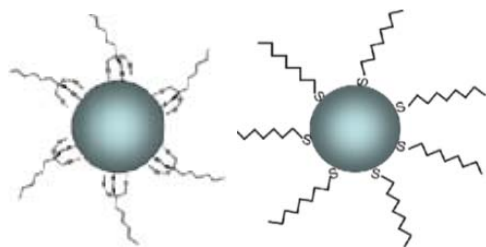
where,  $\beta$  is a decay constant related to the probability of electron tunneling from one gold particle to another,  $s$  is the interparticle distance,  $E_c$  is the activation energy, and  $k_B$  is the Boltzmann constant. The activation energy is given by

$$E_c = \frac{1}{4\pi\epsilon_0\epsilon_r} \frac{e^2}{r} \quad (2)$$

where,  $e$  is the fundamental charge,  $\epsilon_0$  is the vacuum permittivity,  $\epsilon_r$  is the dielectric constant of the film, and  $r$  is the radius of Au nanoparticle. From these relations, it is evident that the nanoparticle size and surface coating play important roles in the sensing performance; thus, significant efforts have been devoted to control the size and surface properties of Au nanoparticles. The distribution and purity of nanoparticles throughout the film are also important considerations. A number of strategies have been developed for synthesizing alkanethiol coated gold nanoparticles films with the aim of achieving monodispersity and low amount of contamination. Other important considerations are the response time and reversibility [24-28].

Despite the promise of thiolated Au nanoparticle-based sensors, there are several problems remaining to be solved, including achieving long-term stability and minimizing signal drift. In practical real-world applications, the sensor must be able to withstand exposure to light, air, and moisture, and perform consistently under conditions producing large fluctuations of temperature and humidity. In several investigations by others and in our own research experience, Au nanoparticle-based sensors were found to begin to lose their sensitivity within few months while operating under ambient condition. This may be largely due to the escape to thiol ligands from the surface of gold [6, 29]. Therefore, a new strategy was needed for making more robust linkages between ligand caps and Au nanoparticles.

With the aim of enhancing particle stability, we designed a new type of ligand containing three thiol groups per molecule to cap Au nanoparticles (Scheme 1). Our rationale is that multiple thiol groups in the ligand will produce much stronger interactions between the ligand and gold core, and hence, the nanoparticle should remain stable for a longer period of time. Indeed, trithiols have been shown to bind more strongly to Au surface compared to monothiols by many authors in their studies involving preparation and applications of self-assembled monolayers (SAMs) and Au nanoparticles [30-32]. Our approach is inspired from the numerous polyvalent interactions that occur throughout biology [33]. The probability of a polyvalent molecule having all thiols simultaneously dissociate from the gold surface (total desorption) is lowered by a power factor of 3, i.e., if the association constant  $K_a = x$  for monothiol ligand, then  $K_a' = x^3$  for trithiol ligand. Herein, we report our work on the synthesis of trithiol-capped Au nanoparticles and their sensing properties when incorporated into chemiresistive sensors. We demonstrate that sensors based on trithiol-capped Au nanoparticles have significantly improved in comparison with those based on monothiol-Au sensors.



**Scheme 1.** Trithiol and monothiol-capped Au nanoparticles.

## 2. Experimental Section

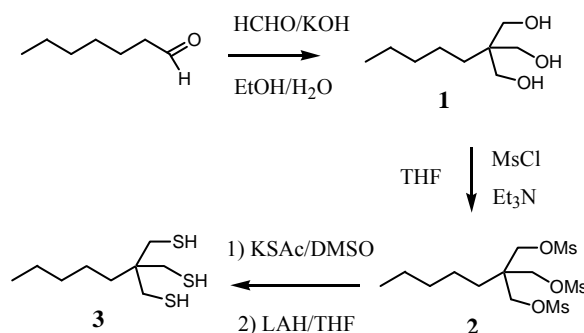
All the reagents were purchased from Sigma-Aldrich and used as received. All aqueous solutions were prepared with Nanopure water (resistivity 18.2 M $\Omega$ ·cm) obtained from a Barnstead NANOpure DIwater system.

### 2.1. Synthesis of 1,1,1-Tris(mercaptomethyl)-hexane (Trithiol)

Heptanal (10 ml, 71.2 mmol) and aqueous formaldehyde (36.5-38.5 %, 40 ml, excess) were dissolved in 50 ml of 50% aqueous ethanol. To this mixture potassium hydroxide (5.7 g, 143.0 mmol) dissolved in 50 ml of 50% aqueous ethanol was added. The mixture was stirred at room temperature for 4 h and then at 60°C for 5 h under a nitrogen atmosphere. The ethanol was then removed by rotary evaporation, and the residue was extracted with hexanes thrice. The combined organic phase was washed with water, dried over MgSO<sub>4</sub> and concentrated to dryness to yield a waxy liquid 1,1,1-tris(hydroxymethyl)hexane (**1**), Scheme 2. The product was purified by column chromatography on silica gel. The impurities were first removed using hexane and the pure product was then eluted using ethyl acetate (3.7 g, yield 30%).

For the next step, compound **1** (3.5 g, 19.8 mmol) and triethylamine (6.0 g, 59.4 mmol) were placed in 75 ml THF under nitrogen atmosphere. To this stirred solution, methanesulfonyl chloride (6.8 g, 59.4 mmol) was added dropwise over a period of ~5 min. The reaction mixture was stirred for ~4 h at room temperature. Ice-cold water (50 ml) was poured into the flask to destroy any remaining methanesulfonyl chloride. The mixture was extracted with hexanes thrice. The combined organic phase was washed sequentially with dilute HCl, water and Na<sub>2</sub>CO<sub>3</sub> solution and water again. The organic layer was dried over MgSO<sub>4</sub>, filtered, and concentrated to dryness to give crude waxy liquid compound 1,1,1-tris(methanesulfonyloxymethyl)hexane (**2**) (5.9 g, yield 90%).

The crude product **2** (4 g, 9.7 mmol) was then dissolved in dry DMSO (20 ml) and potassium thioacetate (5.5 g, 48.5 mmol) was added to the stirred solution, the reaction mixture was heated to 80°C for 24 h under a nitrogen atmosphere. Water (100 ml) was poured into the solution, and the mixture was extracted with hexanes thrice. The combined organic phase was washed with brine, dried over MgSO<sub>4</sub>, and filtered. The solvent was removed by rotary evaporation. The crude product was placed in 20 ml THF and lithium aluminum hydride (2.0 g, 52.7 mmol) was added slowly at room temperature. The reaction mixture was refluxed for 4 h under an atmosphere of nitrogen and then quenched by slow addition of 25 ml ethanol. The mixture was acidified by careful addition of 1 M HCl solution (150 mL) and then extracted with hexanes. The combined organic layers were washed with dilute HCl solution and brine. The organic phase was dried over MgSO<sub>4</sub>, filtered and volatiles were removed using rotary evaporation to yield waxy liquid yellowish product 1,1,1-tris(mercaptomethyl)hexane (trithiol, **3**). The product was purified by column chromatography on silica gel using hexanes as the eluent. The identification and purity was checked by <sup>1</sup>H NMR.



**Scheme 2.** The synthetic route to trithiol **3**.

### 2.2. Synthesis of monothiol coated Au nanoparticles<sup>27</sup>

HAuCl<sub>4</sub>·3H<sub>2</sub>O (0.125 g) was dissolved in 10 ml THF (HPLC grade) and stirred for 10 min under nitrogen. Octanethiol (20  $\mu$ l) was added using a plastic pipette and the solution was stirred for 10 min. NaBH<sub>4</sub> (43 mg, dissolved in 3 ml ice-cold water) was slowly added to the solution (~1 ml/min), followed by the addition of 2 ml of toluene (HPLC grade) and the solution was stirred for 30 min to ensure the completion of the reaction. The resulting solution was washed with water. Then water was removed using a separating funnel.

Purification of product was as follows. Acetonitrile (10ml) was added; the suspension was centrifuged and the supernatant was decanted. Ethanol was added to the precipitate, and the suspension was centrifuged, followed by removal of the supernatant; this procedure

was repeated 3 times. Finally, toluene was added to dissolve the nanoparticles; the solution was centrifuged at 8000 rpm for 15min, followed by removal of precipitates if any. The nanoparticle solution was dried with nitrogen gas stream. The yield of Au nanoparticles is ~ 50% (on an Au basis).

### 2.3. Synthesis of Trithiol coated coated Au nanoparticles

The synthesis of trithiol capped gold nanoparticles was accomplished using a two-phase approach [34].  $\text{HAuCl}_4 \cdot 3\text{H}_2\text{O}$  (0.4 mmol) was dissolved in 5 ml of nanopure water; TOAB (tetraoctylammonium bromide) was dissolved in 10 ml toluene. The two solutions were combined in a 25 ml tri-neck round bottom flask. The solution was vigorously stirred with a magnetic stir bar to facilitate phase transfer of Au(III) salt into toluene phase (under  $\text{N}_2$  atmosphere). After ~15 min, phase transfer was completed, leaving a clear aqueous phase at the bottom of the flask, which was removed using a syringe. Under constant stirring, trithiol ( $\text{C}_{10}\text{H}_{23}\text{S}_3$ , 3 equivalents per mole of gold) was added. The deep red solution turned to faint yellow with 10 min and almost clear within 1 hour. After one hour, an aqueous solution of  $\text{NaBH}_4$  (10 equivalent per mole of gold) was added rapidly all at once. The solution turned dark brown immediately. The solution was stirred for another hour and then UV-vis spectrum was recorded. The crude product was purified by washing with methanol (3 times) to remove TOAB and other side products. The nanoparticles were stored in dry powders prior to use. The yield obtained is 55 % (on an Au basis).

### 2.4. Nanoparticle characterization.

UV-vis spectra were recorded on a Hewlett-Packard (HP) 8453 diode array optical spectrophotometer. Transmission electron microscopy (TEM) imaging was performed on a Hitachi 7100 TEM operated at 75 kV. Thermal gravimetric analysis (TGA) (~ 2 mg sample used) was conducted under a  $\text{N}_2$  atmosphere (flow rate ~50 mL/min) on a TG/DTA6200 analyzer (Seiko Instruments, Inc); the heating rate was 10 C/min.  $^1\text{H}$  NMR spectra was collected on a Bruker Avance 300 MHz spectrometer.

### 2.5. Fabrication of sensors and test procedure.

Gold nanoparticles were dissolved in 1,2,4-trichlorobenzene (TCB) at 10 mg/mL concentration and ink-jetted onto 75 nm thick spiral gold interdigitated electrodes with 250  $\mu\text{m}$  O.D. A custom-built inkjet system with computer vision-based targeting calibration was used to accurately deposit the drops onto the electrodes [35].

Chemiresistances were measured by applying 1V across the electrodes and measuring the current through the device using a Keithley 6485 picoammeter. The chemical sensitivity was determined by pumping liquid analyte into a 1 L/min nitrogen gas stream using an M6 Milligat solvent pump. A brass heater block (heated to 48 °C) was used to evaporate the solvent into the flow-stream. The flow was passed into a 500 mL mixer to improve the uniformity of VOC/ $\text{N}_2$  flow before passing into a test box containing the sensor. The gaseous analyte concentration was controlled by adjusting the relative flow rate of  $\text{N}_2$  and analyte gases using mass controllers.

## 3. Results and Discussion

### 3.1. Synthesis of Au nanoparticles capped by trithiol and monothiol

The as-synthesized monothiol and trithiol capped gold nanoparticles (*abbreviated* as monothiol-Au and trithiol-Au NPs) show surface plasmon resonance at ~520 nm (figure 1), which is characteristic of spherical Au nanoparticles. The less prominent plasmon band indicates the small size of these nanoparticles. TEM analysis shows that both types of nanoparticles have a similar size (3-4 nm), figure 2. NMR spectra reveal that the nanoparticles are free of TOAB surfactant. The purity of nanoparticles is quite important, as previous work by Rowe and coworkers found that the presence of residual TOAB in the nanoparticle sample could interfere with chemical sensing [27]. The high purity of both trithiol-Au and monothiol-Au nanoparticles ensures no interference from impurities.

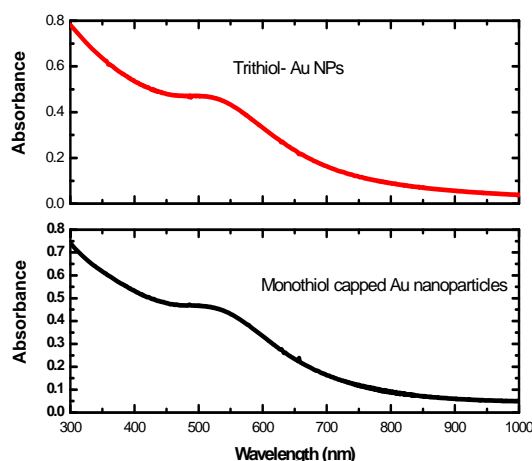


**Figure 1.** UV-vis spectrum for Trithiol and Monthiol capped Au NPs.

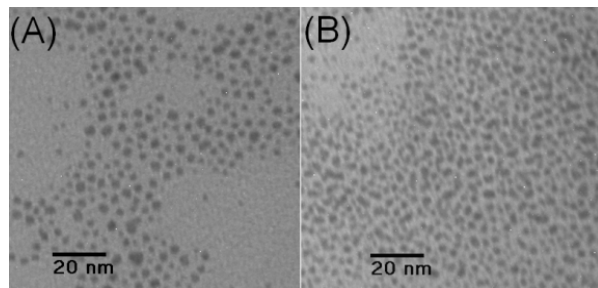


**Figure 2.** TEM image of (A) monothiol capped Au NPs and (B) trithiol capped Au NPs.

### 3.2. VOC sensing properties of Au nanoparticles

The thiol-capped Au nanoparticles were subsequently used for sensor fabrication. The sensors were fabricated by ink-jet deposition of  $\sim 9$  nanoliters Au nanoparticle solution (10 mg/ml in TCB) onto a spiral electrode (figure 3) using a custom-built inkjet deposition system. The sensors were then evaluated for their response to different chemical vapors. We focussed on the trithiol-Au sensor since the monothiol-Au system has previously been extensively studied in literature.

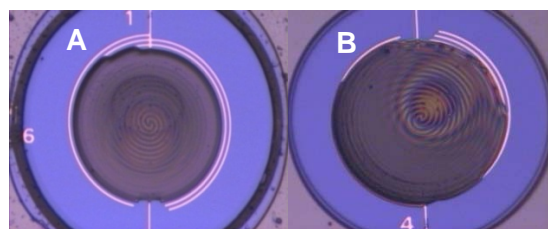


**Figure 3.** Ink-jetted splats on spiral interdigitated electrodes. (A) monothiol-Au NPs, and (B) trithiol-Au NPs.

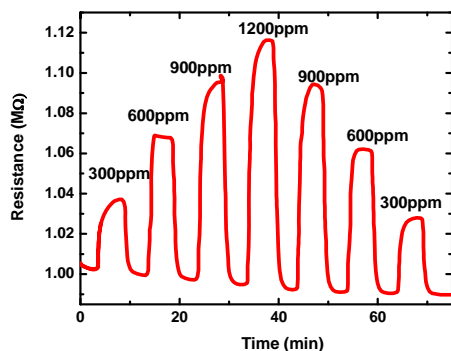


**Figure 4.** Response of trithiol capped Au nanoparticle-based chemiresistive sensor to toluene.

We first test the trithiol-Au sensor response with toluene analyte. Figure 4 shows a linear response of the sensor to different concentrations of toluene (diluted

with  $N_2$ ). In all tests, a high signal-to-noise ratio was observed, indicating excellent response of the sensor to the vapor. In addition, the sensor exhibited a fast response time (few seconds) and a completely reversible response; the latter demonstrates that there was no deterioration caused by analyte sorption/desorption to the nanoparticle thin film.

### 3.3. Comparison of trithiol-Au and monothiol-Au sensors

It is worth comparing the sensitivity of trithiol-Au and monothiol-Au sensors to different types of volatile chemical vapors VOCs, including toluene, ethanol, dichloroethane (DCE), methanol and acetone. The responses of monothiol-Au and trithiol-Au sensors to these vapors, as measured by change in resistance ( $\Delta R/R$ ) are similar, figure 5. The sensors are very sensitive to toluene and moderate to other VOCs.

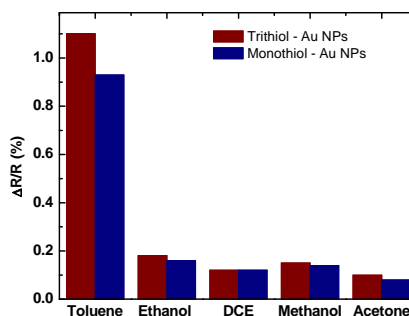


**Figure 5.** Responses of trithiol and monothiol capped Au nanoparticle sensors to various VOCs.

To compare the response linearity, figure 6 shows the sensitivity of the sensors as a function of toluene vapor concentration. Both nanosensor responses are linear; indeed, the trithiol-Au based sensor shows a somewhat higher sensitivity.

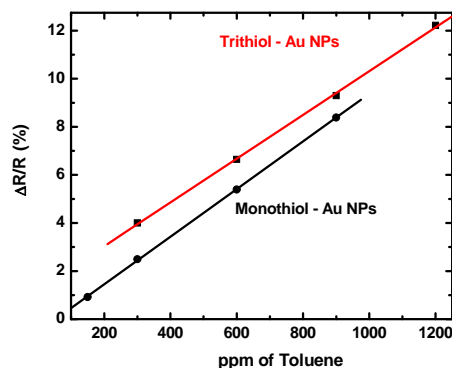


**Figure 6.** Response for varying the concentration of toluene by trithiol and monothiol-Au nanosensors.

The somewhat higher sensitivity of the trithiol-Au nanosensor could be due to two possible causes: 1) cross-linking between the ligands of closely located nanoparticles may occur, which would bring metal cores closer to each other in the thinfilm and hence the probability of electron tunneling within particles would increase; 2) since each trithiol molecule presumably replaces three insulating monothiol molecule, electron hopping will be more effective since relatively less insulating surface would cover the Au surface. TGA results confirm that organic content of trithiol nanoparticles (14%) is lower compared to monothiol nanoparticles (17%).

With respect to the sensor responses to different vapors, multiple mechanisms of charge conduction seem to be operating in terms of charge conduction within the monolayer-coated nanoparticles. When the analyte is adsorbed, a number of factors changes, such as the permittivity of the organic matrix surrounding the metal cores and the spacing between metal cores. Sensing response was found to be greatly dependent on the analyte's physical parameters, including boiling point, dielectric constant and polarizability of the vapor (Table 1). The organic vapors with low boiling point ( $T_b$ ) were found to show a lower response, which could be attributed to relatively less absorption of vapor molecules on the monolayer surface. In the case of alcohols or other polar molecules, the response is lower compared to non-polar VOCs like toluene, which might be due to higher changes in permittivity of the film matrix because of their high dielectric constant. Considering the mechanism of electron tunneling and hopping, polarizability of the analyte should also influence the overall response, however, we did not find any strong correlation in our studies. Also, the reason for the high response of monothiol and trithiol Au nanosensors towards toluene compared to other VOCs is less understood at present.

**Table 1.** Physical properties of various VOCs [36, 37].

Vapor	$T_b$ (°C)	Dielectric constant	Polarizability ( $\text{\AA}^3$ )
Toluene	111	2.4	9.4
Ethanol	78.4	24.3	5.2
DCE	84	10.5	8.35
Methanol	64.7	33.1	5.1
Acetone	56.5	20.7	6.4

### 3.4. Long-term stability of sensors

The long term stability of the nanosensor is a critical consideration for deployment in real world applications. Ideally, a lifetime of the sensor should be at least to 5 years. Previously, we found that the monothiol-Au sensor starts to significantly degrade in less than a year. We expected that the trithiol-Au nanoparticles based sensor devices should have a much higher stability over the monothiol-Au nanoparticles. This is indeed observed in the two types of sensors over a six-month test period. We found that the response of trithiol-Au to a 500 ppm toluene vapor was quite constant with only a small drop in sensitivity (<10%, relative to the fresh sensor's response) over a half period (figure 7). In contrast, the monothiol-Au sensor shows a large drop (~47%) in response. More importantly, the trithiol-Au sensor response became stabilized after approximately 3 months, while the monothiol-Au sensing performance continued to degrade with time. These tests explicitly demonstrated significantly improved long-term stability of the trithiol-Au based nanosensors.

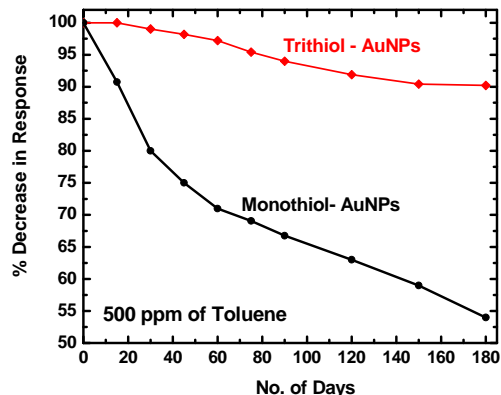


**Figure 7.** Response of trithiol-Au and monothiol-Au based sensors to 500 ppm toluene over a six month test period.

The lower stability of monothiol-Au nanoparticles is likely due to the monothiolate ligands on the particle surface being easier to oxidize under ambient conditions. It is well-known that free thiol molecules (R-SH) are prone to oxidation by  $O_2$  when exposed to air, forming sulfonyl-like oxidized products [38]. In the case of Au-SR nanoparticles, the surface thiolate is less susceptible to oxidation due to binding to gold and the electron-rich nature of the gold core; nevertheless, slow oxidation of the surface thiolate (RS-) still occurs on a time scale of months to one year when exposed to air, light and moisture under ambient conditions. The oxidized ligands can no longer protect the Au core and the sulfonyl species may desorb from the particle surface, hence, aggregation of nanoparticles will occur. The aggregated nanoparticles make the thin-film much

more conductive compared to the fresh thin-film, resulting in severe deterioration of the sensor performance. When the nanoparticles are capped by trithiol ligands, the oxidation process of the thiolate group of the trithiolate ligand still occurs to some extent, however, the deterioration rate should be significantly slower since the chance of three thiolate groups being completely oxidized and desorbed is significantly lower. Thus, aggregation of nanoparticles is largely inhibited. Another possible factor that may contribute to the particular stability of trithiol-Au nanoparticles is the higher binding energy of trithiolate to gold, which remains to be elucidated by X-ray photoelectron spectroscopy in future work.

#### 4. Conclusion

The long term stability of nanoparticle-based sensors is very critical for being able to deploy them in real world applications. In this work, we have demonstrated a successful strategy to increase stability by using trithiol to cap Au nanoparticles. Sensors based on trithiol-Au nanoparticles show excellent response to VOC vapors, and these responses are similar to those of monothiol-Au sensors. The stability of such trithiol-Au sensors, however, is significantly improved compared to monothiol-Au sensors. Thus, sensors made with trithiol-Au nanoparticles hold great potential in monitoring applications such as safety equipments worn by workers in hazardous environment.

**Acknowledgement.** This work is funded in part by NIOSH/CDC (contract 200-2002-00528) and AFOSR grant FA9550-07-1-0245.

#### References

- Zhang, P.; Vincent, A.; Seal, S.; Cho, H. *Proceedings of SPIE* **2009**, 7318.
- Palzer, S.; Moretton, E.; Ramirez, F., H.; Romano-Rodriguez, A.; Woellenstein, J. *Microsystem Technologies* **2008**, 14, 645-651.
- Lu, Y.; Li, J.; Han, J.; Ng, H.-T.; Binder, C.; Partridge, C.; Meyyappan, M. *Chemical Physics Letters* **2004**, 391, 344-348.
- Franke, M. E.; Koplín, T. J.; Simon, U.; *Small* **2006**, 2, 36-50.
- Haick, H.; *J Phys. D: Appl. Phys.* **2007**, 40, 7173-7186.
- Krasteva, N.; Besnard, I.; Guse, B.; Bauer, R. E.; Mullen, K.; Yasuda, A.; Vossmeier, T. *Nano Lett.*, 2002, 2, 551-555.
- Li, B.; Sauve', G.; Iovu, M. C.; Jeffries-EL, M.; Zhang, R.; Cooper, J.; Santhanam, S.; Schultz, L.; Revelli, J. C.; Kusne, A. G.; Kowalewski, T.; Snyder, J. L.; Weiss, L. E. Fedder, G. K.; McCullough, R. D.; Lambeth D.N. *Nano Lett.* **2006**, 6, 1598-1602.
- Ampuero, S.; Bosset, J. O. *Sens. Actuators, B* **2003**, 94, 1-12.
- Snow, E. S.; Perkins, F. K.; Houser, E. J.; Badescu, S. C.; Reinecke, T. L. *Science* **2005**, 307, 1942-1945.
- Srivastava, A. K. *Sens. Actuators, B* **2003**, 96, 24-37
- Valli, L.; *Advances in Colloid and Interface Science*, **2005**, 116, 13-44.
- McCullough, R. D.; Sauve', G.; Li, B.; Jeffries-EL, M.; Santhanam, S.; Schultz, L.; Zhang, R.; Iovu, M. C.; Cooper, J.; Sreedharan, P.; Revelli, J. C.; Kusne, A. G.; Kowalewski, T.; Snyder, J. L.; Weiss, L. E.; Lambeth, D. N.; Fedder, G. K. *Proc. SPIE* **2005**, 5940, 28-34.
- Srivastava, S.; Sharma, S. S.; Agrawal, S.; Kumar, S.; Singh, M.; Vijay, Y. K. *Synthetic Metals* **2010**, 160, 529-534.
- Wohltjen, H.; Snow, A. W. *Anal. Chem.* **1998**, 70, 2856-2859.
- Barash, O.; Peled, N.; Hirsch, F. R.; Haick, H. *Small*, **2009**, 5, 2618-2624.
- Shirsat, M. D.; Bangar, M., A.; Deshusses, M., A.; Myung, N. V.; Mulchandani, A. *Applied Physics Letters* **2009**, 94, 083502/1-083502/3
- Ibanez, F. J.; Zamborini, F. P. *ACS Nano* **2008**, 2, 1543-1552.
- Joseph, Y.; Guse, B.; Vossmeier, T.; Yasuda, A. *J. Phys. Chem. C* **2008**, 112, 12507-12514.
- Steinecker, W. H.; Rowe, M. P.; Zellers, E. T. *Anal. Chem.* **2007**, 79, 4977-4986.
- Ancona, M. G.; Snow, A. W.; Foos, E. E.; Kruppa, W.; Bass, R. *IEEE Sensors Journal* **2006**, 6, 1403-1414.
- Joseph, Y.; Besnard, I.; Rosenberger, M.; Guse, B.; Nothofer, H. G.; Wessels, J.; Wild, U.; Knop-Gericke, A.; Su, D.; Yasuda, A.; Vossmeier, T. *J. Phys. Chem. B* **2003**, 107, 7406-7413.
- Andres, R. P.; Bielefeld, J. D.; Janes, D. B.; Kolagunta, V. R.; Kubiak, C. P.; Mahoney, W. J.; Osifchin, R. G. *Science* **1996** 273, 1690-1693.
- Wuelfing, W. P.; Green, S. J.; Pietron, J. J.; Cliffel, D. E.; Murray, R. W. *J. Am. Chem. Soc.* **2000**, 122, 11465-11472.
- Joseph, Y.; Guse, B.; Vossmeier, T.; Yasuda, A. *J. Phys. Chem. C*, **2008**, 112, 12507-12514.
- Joseph, Y.; Peic, A.; Chen, X.; Michl, J.; Vossmeier, T.; Yasuda, A. *J. Phys. Chem. C* **2007**, 111, 12855-12859.
- Trudeau, P. E.; Kwan, E.; Orozco, A.; Dhirani, A.-A. *J. Chem. Phys.* **2002**, 117, 3978-3981.
- Rowe, M. P.; Plass, K. E.; Kim, K.; Kurdak, Ç.; Zellers, E. T.; Matzger A. *J. Chem. Mater.* **2004**, 16, 3513-3517.
- Brust, M.; Walker, M.; Bethell, D.; Schiffrin, D. J.; Whyman, R. *J. Chem. Soc., Chem. Commun.* **1994**, 801-802.
- Cai, Q.-Y.; Zellers E. T. *Anal. Chem.* **2002**, 74, 3533-3539.
- Park, J. S.; Vo, A. N.; Barriet, D.; Shon, Y.-S.; Lee, T. R. *Langmuir* **2005**, 21, 2902-2911.
- Wojczykowski, K.; Meibner, D.; Jutzi, P.; Ennen, I.; Hutten, A.; Fricked, M.; Volkmer, D. *Chem. Commun.*, **2006**, 3693-3695.
- Wang, W.; Zhang, S.; Chinwangso, P.; Advincula, R. C.; Lee, T. R. *J. Phys. Chem. C* **2009**, 113, 3717-3725.
- Mammen, M.; Choi, S.; Whitesides, G. M. *Angew. Chem. Int. Ed.* **1998**, 37, 2754-2794.

34. Zhu, M.; Lanni, E.; Garg, N.; Bier, M. E.; Jin, R. *J. Am. Chem. Soc.* **2008**, *130*, 1138–1139.
35. Weiss, L. E.; Schultz, L.; Miller E.; **2006**, CMU-RI-TR-06-15.
36. Wyman, J. Jr. *J. Am. Chem. Soc.* **1936**, *58*, 1482–1486.
37. Bosque, R.; Sales J. *J. Chem. Inf. Comput. Sci.*, **2002**, *42*, 1154–1163.
38. Schoenfisch, M. H.; Pemberton, J. E. *Am. Chem. Soc.* **1998**, *120*, 4502–4513.